4076 *Chem. Mater.* **2010,** *22,* 4076–4082
DOI:10.1021/cm100960g

CHEMISTRY OF MATERIALS
Article

Energy-Efficient, High-Color-Rendering LED Lamps Using Oxyfluoride and Fluoride Phosphors

Anant A. Setlur,*[,†,‡] Emil V. Radkov,[§,†,#] Claire S. Henderson,[‡] Jae-Hyuk Her,[‡] Alok M. Srivastava,[‡] Nagaveni Karkada,[⊥] M. Satya Kishore,[⊥] N. Prasanth Kumar,[⊥] Danny Aesram,[§] Anirudha Deshpande,[§] Boris Kolodin,[§] Ljudmil S. Grigorov,[||] and Uwe Happek[▽]

[‡]*GE Global Research, 1 Research Circle, Niskayuna, New York 12309,* [§]*GE Lighting Solutions, 1975 Noble Road, East Cleveland, Ohio 44112,* [⊥]*GE Global Research, Hoodi Village, Whitefield Road, Bangalore 560066, India,* [||]*Scientific Research Department, University of Sofia, 8 Dragan Tzankov Avenue, 1164 Sofia, Bulgaria, and* [▽]*Department of Physics and Astronomy, University of Georgia, Athens, Georgia 30602.* [†] *These authors contributed equally to this work.* [#] *Current address: Illumitex, 5307 Industrial Oaks Blvd., Austin, TX 78735.*

Received April 6, 2010. Revised Manuscript Received May 24, 2010

LED lamps using phosphor downconversion can be designed to replace incandescent or halogen sources with a "warm-white" correlated color temperature (CCT) of 2700−3200 K and a color rendering index (CRI) greater than 90. However, these lamps have efficacies of ∼70% of standard "cool-white" LED packages (CCT = 4500−6000 K; CRI = 75−80). In this report, we describe structural and luminescence properties of fluoride and oxyfluoride phosphors, specifically a $(Sr,Ca)_3(Al,Si)O_4(F,O):Ce^{3+}$ yellow-green phosphor and a $K_2TiF_6:Mn^{4+}$ red phosphor, that can reduce this gap and therefore meet the spectral and efficiency requirements for high-efficacy LED lighting. LED lamps with a warm-white color temperature (3088 K), high CRI (90), and an efficacy of ∼82 lm/W are demonstrated using these phosphors. This efficacy is ∼85% of comparable cool-white lamps using typical $Y_3Al_5O_{12}:Ce^{3+}$-based phosphors, significantly reducing the efficacy gap between warm-white and cool-white LED lamps that use phosphor downconversion.

1. Introduction

Typical high efficacy LED lamps are based upon phosphor downconversion of blue InGaN LEDs by $Y_3Al_5O_{12}:Ce^{3+}$ (YAG:Ce)-based yellow phosphors.[1−4] The combination of yellow YAG:Ce emission and blue LED radiation that bleeds through a YAG:Ce coating gives "cool"-white light with correlated color temperature (CCT) greater than ∼4000 K and color rendering index (CRI) values of 70−80. However, the need to replace incandescent and halogen lamps with "warm"-white LEDs with lower CCTs of 2700−3200 K has driven LED phosphor development toward compositions beyond the Ce^{3+}-doped garnets used in cool-white LED packages. One focus has been on Ce^{3+}/Eu^{2+}-doped (oxy)nitride phosphor compositions whose emission can cover the entire visible spectrum.[5−9] The energy of Eu^{2+}/Ce^{3+} $4f^N \rightarrow 4f^{N-1}5d^1$ transitions can be lowered by more covalent Eu^{2+}/Ce^{3+}−ligand bonds and higher anion polarizabilities,[10] generally making (oxy)nitride phosphors more likely to strongly absorb violet/blue InGaN LED radiation and emit in the green and red spectral regions. This reasoning has led to efficient Eu^{2+}-doped (oxy)nitride phosphors[5−9] including the red phosphors required for warm-white lamps; (oxy)nitride phosphor blends can give warm-white phosphor converted LEDs with CRI values greater than 90.[8,9]

However, the bandwidth of red Eu^{2+} $4f^6 5d^1 \rightarrow 4f^7$ emission (FWHM >70 nm) reduces the luminous efficacy of radiation (LER), given in units of lumens per watt of radiometric power (lm/W_{rad}), because these phosphors have a significant deep red intensity that does not match the human eye sensitivity well. As an example, lamps that could meet the U.S. DOE L-Prize CCT and CRI requirements (CCT = 2700−3000K; CRI > 90) with YAG:Ce yellow phosphors and deep red nitride phosphors[7]

*Corresponding author. E-mail: setlur@ge.com.

(1) *Multi-Year Program Plan FY'09-FY'15: Solid-State Lighting Research and Development*; Office of Energy Efficiency and Renewable Energy, U.S. Department of Energy: Washington, D.C., 2009.
(2) Phillips, J. M.; Coltrin, M. E.; Crawford, M. H.; Fischer, A. J.; Krames, M. R.; Mueller-Mach, R.; Mueller, G. O.; Ohno, Y.; Rohwer, L. E. S.; Simmons, J. A.; Tsao, J. Y. *Laser Photon. Rev.* **2007**, *1*, 307.
(3) Nakamura, S. *MRS Bull.* **2009**, *34*, 101.
(4) Schubert, E. F.; Kim, J. K. *Science* **2005**, *308*, 1274.
(5) Li, Y. Q.; van Steen, J. E. J.; van Krevel, J. W. H.; Botty, G.; Delsing, A. C. A.; DiSalvo, F. J.; de With, G.; Hintzen, H. T. *J. Alloys Compd.* **2006**, *417*, 273.
(6) Bachmann, V.; Jüstel, T.; Meijerink, A.; Ronda, C.; Schmidt, P. J. *J. Lumin.* **2006**, *121*, 441.
(7) Uheda, K.; Hirosaki, N.; Yamamoto, Y.; Naito, A.; Nakajima, T.; Yamamoto, H. *Electrochem. Solid-State Lett.* **2006**, *9*, H22.
(8) Mueller-Mach, R.; Mueller, G.; Krames, M. R.; Höppe, H. A.; Stadler, F.; Schnick, W.; Juestel, T.; Schmidt, P. *Phys. Status Solidi A* **2005**, *202*, 1727.
(9) Kimura, N.; Sakuma, K.; Hirafune, S.; Asano, K.; Hirosaki, N.; Xie, R.-J. *Appl. Phys. Lett.* **2007**, *90*, 051109.
(10) Dorenbos, P. *Phys. Rev. B* **2002**, *65*, 235110.

 Published on Web 06/04/2010

($\lambda_{max} \approx 640-655$ nm) have a LER of 280−295 lm/W_{rad} versus ~340 lm/W_{rad} for "cool"-white lamps (CCT = 5000 K) with YAG:Ce. These LER differences are a key factor behind the efficacy gap between typical cool-white and warm-white LEDs, and an efficacy gap of ~30% has been projected for the practical maximum package efficacy of cool-white and warm-white LEDs (228 and 162 $lm/W_{electrical}$, correspondingly).[1]

Considering covalency and anion polarizability arguments in the development of LED phosphors alone, fluoride and oxyfluoride hosts would normally be excluded due to the ionic nature of metal−F^- bonds, limiting compositional spaces when screening for new phosphor compositions. However, the study of unconventional systems sometimes leads to desirable properties outside of typical expectations. One recent example for oxyfluoride-based phosphors has been for $(Sr,Ba)_3AlO_4F:Ce^{3+}$, which shows efficient blue-green Ce^{3+} emission under violet excitation.[11−14] In this report, we expand upon this work by describing fluoride and oxyfluoride compositions, specifically a $(Sr,Ca)_3(Al,Si)O_4(O,F):Ce^{3+}$ yellow-green phosphor and a $K_2TiF_6:Mn^{4+}$ red phosphor,[15,16] that meet efficacy and color-quality targets for future SSL lamps. The combination of yellow-green Ce^{3+} emission and narrow-line red Mn^{4+} emission leads to high CRI lamps without LER penalties. These phosphors also have quantum efficiencies (QEs) that are comparable to commercial Ce^{3+}-doped garnets at room temperature, and the efficiency does not deteriorate at elevated temperatures, an important aspect for system efficacy due to elevated LED, package, and luminaire temperatures.[1,2] Consequently, LED lamps using these phosphors have a combination of high efficacies (> 80 lm/W), warm-white CCTs (~3000 K), and high CRIs (~90). These phosphor systems reduce the efficacy gap between high-CRI, warm-white LEDs and cool-white LEDs[1] and can potentially fulfill efficacy and color-quality requirements for future lighting systems.

2. Experimental Procedure

$(Sr,Ca)_3(Al,Si)O_4(O,F):Ce^{3+}$ phosphors are made using typical solid-state routes by initially blending $SrCO_3$ (Aldrich), $CaCO_3$ (Aldrich), CeO_2 (Alfa Aesar), Na_2CO_3 (Fisher), α-Al_2O_3 (Ceralox), fumed silica (Cabosil), and SrF_2 (Aldrich) powders using ZrO_2 media. Excess SrF_2 is used as a flux to increase phosphor quantum efficiency. This powder mixture is initially fired at 750−950 °C in N_2/H_2 mixtures, reground, and refired at 1200−1300 °C in N_2/H_2 mixtures. Typical samples are then wet-milled in isopropanol to a median particle size of ~15−20 μm, as measured by light scattering (Horiba LA-920). The procedure to make $K_2TiF_6:Mn^{4+}$ or $K_2SiF_6:Mn^{4+}$ starts with the synthesis of K_2MnF_6 by Bode's method.[17] K_2MnF_6 and the host fluoride (Aldrich) are then dissolved in 70% HF in Teflon beakers with the nominal Mn^{4+} concentration ranging from 3 to 8%, replacing either Ti^{4+} or Si^{4+}. Phosphor powders are made by cocrystallization after evaporating the solvent at 70 °C. (Warning: Concentrated HF is highly hazardous and should be handled with extreme care.) These powders are dry-milled to a median particle size of ~15−20 μm.

Steady-state photoluminescence measurements used a SPEX Fluorolog 3 with a Xe lamp source; the detection system was calibrated using a NIST-traceable tungsten-halogen lamp. Relative quantum efficiency measurements are corrected for the sample absorption using a $BaSO_4$ (Kodak) powder reflectance standard that has a reflectance of ~95% across the visible and ultraviolet spectrum. The phosphor standard used in these measurements is a YAG:Ce composition (GE Lighting) with 2−3% Ce^{3+}. The errors in the relative plaque QE measurements are ±3% as determined by measuring the same sample on multiple occasions. Intensity measurements at high temperatures used powder samples pressed into an Al plaque with cartridge heaters and a thermocouple that is interfaced into a Watlow temperature controller. The errors in the intensity quenching measurements are ±2%.

Time-resolved measurements at elevated temperatures used a LED excitation source filtered through a narrow band interference filter (10 nm width) driven by the amplified (Avantec) pulses of an Avtech AVP-C pulse generator. The emission was filtered through a 0.5 m McPherson monochromator and detected with a Hamamatsu R212 PMT detector. The time-resolved fluorescence was recorded through a photon counting system, consisting of an Ortec 567 time-to-amplitude converter in conjunction with an EG&G pulse height analyzer. The temporal response for this experimental setup was measured at 2 ns. Unless specifically mentioned, all luminescence measurements are at room temperature.

X-ray diffraction experiments used samples that were additionally ground and passed through a 20 μm sieve. Initial X-ray powder diffraction (XRPD) data were obtained at ambient conditions with a Bruker D8 Advanced sealed tube diffractometer in reflection geometry (1.6 kW, Cu Kα radiation). To achieve a better powder-averaged signal, the sample was rotated during data collection, where the axis is perpendicular to the theta and momentum transfer direction. Since the differences between two possible structure types for $(Sr,Ca)_3(Al,Si)O_4(O,F):Ce^{3+}$, Sr_3SiO_5 (space group *P*4/*ncc*; no. 130) and Sr_3AlO_4F (space group *I*4/*mcm*; no. 140) are small, we used the X14A beamline at the National Synchrotron Light Source (NSLS), Brookhaven National Laboratory, for high-resolution XRPD. The X-ray beam was horizontally focused by a sagittal focusing Si(111) monochromator and vertically focused by a high-performance grazing incidence mirror. The beam size after the incidence slit was 0.5 mm × 1.5 mm. The X-ray wavelength was set to 0.77442(3) Å. The sample was loaded into a 0.3 mm thin-wall quartz capillary and spun during data collection for better powder-averaged signals. A 640-channel Si strip detector, placed at 1433 mm from the sample filled capillary, was used to measure the diffracted intensity. The typical counting time for a full powder diffraction pattern is about 5 min.

Phosphor-coated glass domes are made by first incorporating $(Sr_{0.595}Ca_{0.4}Ce_{0.005})_3Al_{0.6}Si_{0.4}O_{4.415}F_{0.585}$ and $K_2TiF_6:Mn^{4+}$ into a two-part methyl silicone binder (Momentive Performance Materials) with *t*-butyl acetate added to thin the phosphor/silicone dispersion. This dispersion is then spray-coated onto 2 cm diameter glass domes using high-pressure air to create an aerosol.

(11) Im, W. B.; Fourré, Y.; Brinkley, S.; Sonoda, J.; Nakamura, S.; DenBaars, S. P.; Seshadri, R. *Opt. Express* **2009**, *17*, 22673.
(12) Im, W. B.; Brinkley, S.; Hu, J.; Mikhailovsky, A.; DenBaars, S. P.; Seshadri, R. *Chem. Mater.* **2010**, *22*, 2482.
(13) Fang, Y.; Li, Y. Q.; Qiu, T.; Delsing, A. C. A.; de With, G.; Hintzen, H. T. *J. Alloys Compd.* **2010**, *496*, 614.
(14) Chen, W.; Liang, H.; Ni, H.; He, P.; Su, Q. *J. Electrochem. Soc.* **2010**, *157*, J159.
(15) Paulusz, A. G. *J. Electrochem. Soc.* **1973**, *120*, 942.
(16) Radkov, E. V.; Grigorov, L. S.; Setlur, A. A.; Srivastava, A. M. U.S. Patent 7 497 973, 2009.
(17) Bode, H.; Jensen, H.; Bandte, F. *Angew. Chem.* **1953**, *65*, 304.

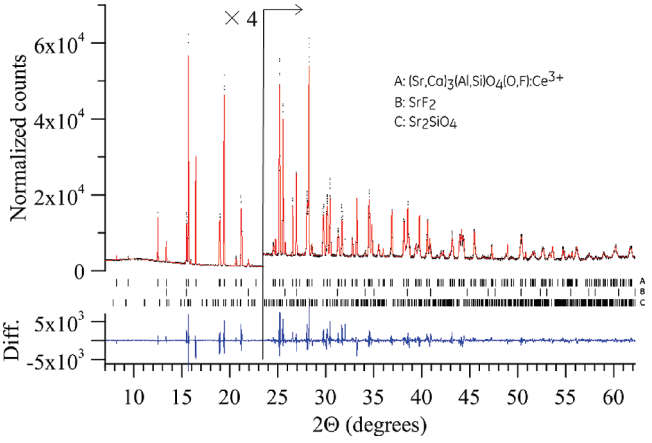

Figure 1. High-resolution synchrotron powder diffraction data (•) and Rietveld fit for the refined structure of $(Sr_{0.5925}Ca_{0.4}Ce_{0.0075})_3Al_{0.6}Si_{0.4}O_{4.4225}F_{0.5775}$ (−). The short vertical lines indicate the positions of the allowed Bragg reflections for the main and secondary phases. The lower trace is a difference plot (measured − calculated), plotted to the same vertical scale.

LED lamps were made using 2 cm diameter phosphor-coated glass domes that were attached to a printed circuit board that has three packaged InGaN LEDs (Nichia) with a peak wavelength of ~450 nm and a wall plug efficiency (WPE) of 45% (350 mA drive current, pulsed operation) in a remote phosphor configuration.[18,19] Measurements of lamp efficacy and color used an integrating sphere calibrated for intensity and spectral response with a NIST-traceable tungsten-halogen lamp.

3. Results and Discussion

3.1. Structural Characterization of $(Sr,Ca)_3(Si,Al)O_4$-(F,O) Phosphors. In our $(Sr_{1-x-y}Ca_xCe_y)_3Al_{1-z}Si_zO_{4+3y+z}$-$F_{1-3y-z}$ X-ray powder diffraction (XRPD) patterns, typically two impurity phases were identified, SrF_2 and Sr_2SiO_4 (Figure 1). The concentration of these impurity phases were ~2 wt % until $x > 0.5$ and $z > 0.5$. Beyond this approximate limit for combined Ca^{2+} and Si^{4+}/O^{2-} substitutions, a significant concentration of $(Sr,Ca)_2SiO_4$ (>5% by weight) is detected in our XRPD patterns. Initially, we also investigated oxygen-rich compositions such as $Sr_3Al_{1-x}Si_xO_{4+x}$-F_{1-x}:Ce^{3+}, where $x > 0.7$. However, because of stronger thermal quenching of Ce^{3+} luminescence in these compositions (vide infra), we did not investigate oxygen-rich compositions in depth. There was a systematic absence of (0*kl*) peaks with odd *k* in initial experimental XRPD data for $(Sr_{1-x-y}Ca_xCe_y)_3Al_{1-z}Si_zO_{4+3y+z}F_{1-3y-z}$ samples with $x < 0.5$ and $z < 0.5$. The absence of these peaks in these samples led to the assumption that their space group was the higher symmetry space group of *I*4/*mcm* (similar to Sr_3AlO_4F[20]), instead of *P*4/*ncc* (similar to Sr_3SiO_5[21,22]). For oxygen-rich $Sr_3Al_{1-x}Si_xO_{4+x}F_{1-x}$:$Ce^{3+}$ ($x > 0.7$) samples, the space group of these materials could be *P*4/*ncc*, but further investigation is necessary for this assignment.

Table 1. Crystallographic Details for $(Sr_{0.5925}Ca_{0.4}Ce_{0.0075})_3Al_{0.6}Si_{0.4}O_{4.4225}F_{0.5775}$

formula	$(Sr_{0.5925}Ca_{0.4}Ce_{0.0075})_3Al_{0.6}Si_{0.4}O_{4.4225}F_{0.5775}$
FW	1264.571
cryst syst	tetragonal
space group	*I*4/*mcm*
a (Å)	6.6603(1)
b (Å)	6.6603(1)
c (Å)	10.8292(1)
α (deg)	90
β (deg)	90
γ (deg)	90
V, (Å^3)	480.37(1)
Z	4
D_{calcd} (g cm^{-3})	4.3713(1)
λ, (Å)	0.77442(3)
$2\theta_{max}$ (deg)	62.25
R_{exp} (%)	2.411
R_{wp} (%)	6.920
GOF	2.870

Table 2. Fractional Coordinates from the Rietveld Refinement of $(Sr_{0.5925}Ca_{0.4}Ce_{0.0075})_3Al_{0.6}Si_{0.4}O_{4.4225}F_{0.5775}$[a]

	Wyckoff site	occ.	*x*	*y*	*z*	*B*
Sr1	4*a*	1	0	0	0.25	0.78(2)
Sr2	8*h*	0.38875	0.1727(1)	0.6727(1)	0	0.60(2)
Ca2	8*h*	0.6	0.1727(1)	0.6727(1)	0	0.60(2)
Ce2	8*h*	0.01125	0.1727(1)	0.6727(1)	0	0.60(2)
Al3	4*b*	0.6	0	0.5	0.25	0.51(4)
Si3	4*b*	0.4	0	0.5	0.25	0.51(4)
O4	16*l*	1	0.1379(3)	0.6379(3)	0.6478(2)	0.86(5)
F5	4*c*	0.5775	0	0	0	1.59(8)
O5	4*c*	0.4225	0	0	0	1.59(8)

[a] Bond lengths: Sr1−O4, 2.808(1) Å (8×); Sr1−(F,O)5, 2.7073(1) Å (2×); (Sr,Ca,Ce)2−O4, 2.397(2) Å (2×); (Sr,Ca,Ce)2−O4, 2.626(2) Å (4×); (Sr,Ca,Ce)2−(F,O)5, 2.4648(2) Å (2×); (Al,Si)3−O4, 1.706(2) Å (4×).

Since the symmetry of the *I*4/*mcm* space group is lowered to the *P*4/*ncc* space group by a displacement of the tetrahedral oxygen anion, the unique reflections in the *P*4/*ncc* space group are weak and more difficult to detect with typical laboratory X-ray sources. However, synchrotron X-ray diffraction experiments for a $(Sr_{0.5925}Ca_{0.4}Ce_{0.0075})_3$-$Al_{0.6}Si_{0.4}O_{4.4225}F_{0.5775}$ sample also showed no additional (0*kl*) peaks with odd *k* that are allowed only in the *P*4/*ncc* space group, so we used the higher symmetry space group of *I*4/*mcm* for the structure refinement of this sample.

The Rietveld refinement of a sample with a nominal composition of $(Sr_{0.5925}Ca_{0.4}Ce_{0.0075})_3Al_{0.6}Si_{0.4}O_{4.4225}$-$F_{0.5775}$ was done using the TOPAS program (Figure 1 and Tables 1 and 2) with additional impurity phases of SrF_2 (2.2(1) wt %) and Sr_2SiO_4 (1.8(2) wt %) included in the refinement. The fractional occupancies of each element were fixed at the nominal composition for charge balance, and the same isotropic displacement parameter (IDP) was used for atoms located on the same site. Additional elemental analysis and/or neutron diffraction is necessary to confirm the exact phosphor composition, especially the fluorine level. The refinement was further constrained by making Ca^{2+} ions only occupy the 8-coordinated 8*h* site (Table 2) as in $(Sr,Ca)_3AlO_4F$.[20] The structure refinement supports the assignment of the space group of $(Sr_{0.5925}Ca_{0.4}Ce_{0.0075})_3Al_{0.6}Si_{0.4}O_{4.4225}F_{0.5775}$ to *I*4/*mcm* through a comparison of the structure models for

(18) Narendran, N.; Gu, Y.; Freyssinier-Nova, J. P.; Zhu, Y. *Physica status solidi* (*a*) **2005**, *202*, R60.
(19) Soules, T. F.; Weaver, S.; Hsing, C.-L.; Kolodin, B.; Sommers, M.; Setlur, A. A.; Stecher, T. E. U.S. Patent 7 479 662, 2009.
(20) Prodjosantoso, A. K.; Kennedy, B. J.; Vogt, T.; Woodward, P. M. *J. Solid State Chem.* **2003**, *172*, 89.
(21) Mansmann, M. *Z. Anorg. Allge. Chem.* **1965**, *339*, 52.
(22) Jang, H. S.; Jeon, D. Y. *Appl. Phys. Lett.* **2007**, *90*, 041906.

the *I*4/*mcm* and *P*4/*ncc* space groups. The refinement using the *I*4/*mcm* space group has a significantly lower R_{wp} (6.920%) versus the refinement for the *P*4/*ncc* space group (R_{wp} = 10.614%). All of the bond lengths for the Sr1 and (Sr,Ca,Ce)2 cations (Table 2) in this material are all smaller than the Sr−O bond lengths in Sr_3AlO_4F,[20] and the cell parameters (Table 1) are also significantly reduced versus Sr_3AlO_4F[20] (a = 6.7822(1) Å and c = 11.1437(2) Å). Both of these results are as expected given the presence of smaller Ca^{2+} and Si^{4+} cations. In addition, taking the tetrahedral bond lengths in Sr_2CaAlO_4F[20](1.760(4) Å) and Sr_3SiO_5[21] (1.639 Å) and a Vegard's law-like estimate, the tetrahedral bond length in $(Sr_{0.5925}Ca_{0.4}Ce_{0.0075})_3Al_{0.6}Si_{0.4}O_{4.4225}F_{0.5775}$ is estimated at 1.711 Å, in good agreement with the refined (Al,Si)-3−O4 bond length of 1.706(2) Å. The tetrahedral bond strain, defined by the deviation in O4-(Al,Si)−O4 bond angles (114.1(1) and 99.1(1)°) from the ideal tetrahedral bond angle of 109.5°, is also comparable to the values in $(Sr,Ba,Ca)_3AlO_4F$.[20] These experiments show no evidence for ordering, but further work could be necessary to understand the local environment and potential ordering as has been done for Sr_2LaAlO_5.[23]

3.2. Luminescence of (Sr,Ca)$_3$(Si,Al)O$_4$(F,O) Phosphors. The $(Sr,Ca)_3Al_{1-x}Si_xO_{4+x}F_{1-x}:Ce^{3+}$ host with $x < 0.5$ is isostructural to other hosts where Ce^{3+} luminescence has been reported such as $(Sr,Ba)_3AlO_4F$,[11−14] $Sr_2(La,Gd)AlO_5$,[13,23,24] and solid solutions of $Sr_2(La,Gd)AlO_5$ with Sr_3SiO_5[25] and Sr_3AlO_4F.[11] One structural feature in these hosts is that the 4c anion is bonded only to larger $Sr^{2+}/Ca^{2+}/RE^{3+}$ cations and is not coordinated by Si^{4+}/Al^{3+} cations. In pure oxide hosts, these anions that are coordinated to only larger cations have been called "free" O^{2-} anions and have a strong effect on RE^{3+} luminescent properties.[26] For example, hosts with "free" O^{2-} anions generally have strong thermal quenching of Ce^{3+} luminescence that has been assigned to Ce^{3+} $5d^1$ ionization.[26,27] This is one possible reason for strong thermal quenching (> 50% QE loss at 150 °C) in $Sr_2(La,Gd)AlO_5$:Ce^{3+}[13,24] and Ce^{3+}-doped $Sr_2(La,Gd)AlO_5$−Sr_3SiO_5 solid solutions.[25] One potential route to reduce ionization-based quenching in hosts with "free" O^{2-} anions would be to increase the host bandgap by substituting F^- for these "free" O^{2-} anions with appropriate charge compensation. The Cs_3CoCl_5 structural family enables this substitution since "free" O^{2-} anions can be completely substituted by F^- in Sr_3AlO_4F.[20] This initial reasoning is supported by the reduced Ce^{3+} luminescence quenching in Sr_3AlO_4F:Ce^{3+}, which has < 15% loss in QE at 150 °C (Figure 2).

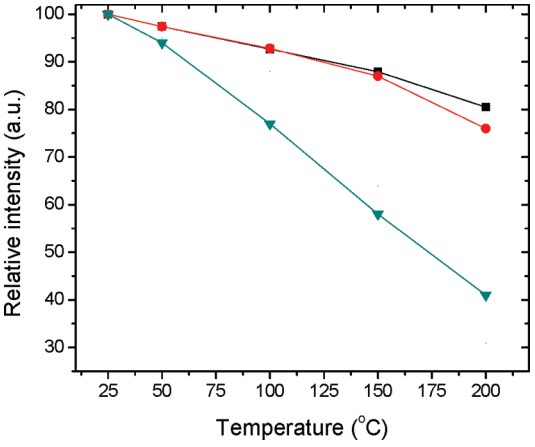

Figure 2. (a) Integrated intensity versus temperature (λ_{ex} = 405 nm) for $(Sr_{0.98}Na_{0.01}Ce_{0.01})_3AlO_4F$ (squares), $(Sr_{0.595}Ca_{0.4}Ce_{0.005})_3Al_{0.6}Si_{0.4}O_{4.415}F_{0.585}$ (circles), and $(Sr_{0.98}Na_{0.01}Ce_{0.01})_3Al_{0.25}Si_{0.75}O_{4.75}F_{0.25}$ (triangles). The drawn lines in the figure are only to guide the eye.

Similar results reporting the reduced thermal quenching in $(Sr,Ba)_3AlO_4F:Ce^{3+}$ versus other Cs_3CoCl_5-based phosphors were also reported during the preparation of this report.[12]

To redshift the near-UV excitation and blue-green emission of $Sr_3AlO_4F:Ce^{3+}$ ($\lambda_{max} \approx 480-500$ nm)[11−14] to more useful spectral regions at low Ce^{3+} concentrations,[14] we replace Sr^{2+} by Ca^{2+} and/or Al^{3+}/F^- by Si^{4+}/O^{2-}. We expect a redshift in the Ce^{3+} emission and excitation spectra from combined Ca^{2+} and Si^{4+}/O^{2-} substitutions due to a combination of stronger Ce^{3+} $5d^1$ crystal field splitting from smaller bond lengths when substituting smaller Ca^{2+}/Si^{4+} ions for Sr^{2+}/Al^{3+} as well as a higher Ce^{3+}−ligand covalency and anion polarizability from the replacement of F^- by O^{2-}.[10,12] As expected, the replacement of Al^{3+}/F^- by Si^{4+}/O^{2-} leads to a lower energy for the lowest energy Ce^{3+} absorption and emission bands (Figure 3a). The drawback when only replacing Al^{3+}/F^- with Si^{4+}/O^{2-} is the strong thermal quenching for Ce^{3+} luminescence at high Si^{4+}/O^{2-} levels (Figure 2). In contrast, combining Ca^{2+} substitution with lower levels of Si^{4+}/O^{2-} substitution can shift and tune the Ce^{3+} emission and excitation (Figure 3b) without significant thermal quenching penalties (Figure 2). These results qualitatively fit into our explanation of Ce^{3+} ionization quenching in these materials since there should be a larger barrier for ionization when F^- substitutes for "free" O^{2-} anions. Also, there does not appear to be a relationship between the position of the Ce^{3+} $5d^1$ level and/or apparent Stokes shift (Figure 3) with the thermal quenching (Figure 2), an indication that nonradiative level crossing is not the key quenching mechanism in these phosphors. An additional factor that can increase barriers for Ce^{3+} $5d^1$ thermal ionization in these compositions is an effective positive charge on Ce^{3+} when it replaces Sr^{2+}/Ca^{2+}.[28] However, if improvements in thermal quenching were mainly due to an effective positive charge on Ce^{3+}, there should be only small differences between O^{2-}-rich and F^--rich compositions, in contrast to our experimental results (Figure 2). Given the similar thermal

(23) Im, W. B.; Page, K.; DenBaars, S. P.; Seshadri, R. *J. Mater. Chem.* **2009**, *19*, 8761.
(24) Srivastava, A. M.; Setlur, A. A.; Comanzo, H. A.; Happek, U.; Hughes, J.; Hannah, M. E. *210th Meeting of the Electrochemical Society Extended Abstracts*; Cancun, Oct 29−Nov 3, 2006; The Electrochemical Society: Pennington, NJ, 2006; p 2172.
(25) Im, W. B.; Fellows, N. N.; DenBaars, S. P.; Seshadri, R. *J. Mater. Chem.* **2009**, *19*, 1325.
(26) Dirksen, G. J.; Blasse, G. *J. Alloys Compd.* **1993**, *191*, 121.
(27) Srivastava, A. M.; Setlur, A. A.; Comanzo, H. A.; Gao, Y.; Hannah, M. E.; Hughes, J. A.; Happek, U. *Opt. Mater.* **2008**, *30*, 1499.
(28) Blasse, G.; van den Heuvel, G. P. M. *J. Lumin.* **1975**, *11*, 47.

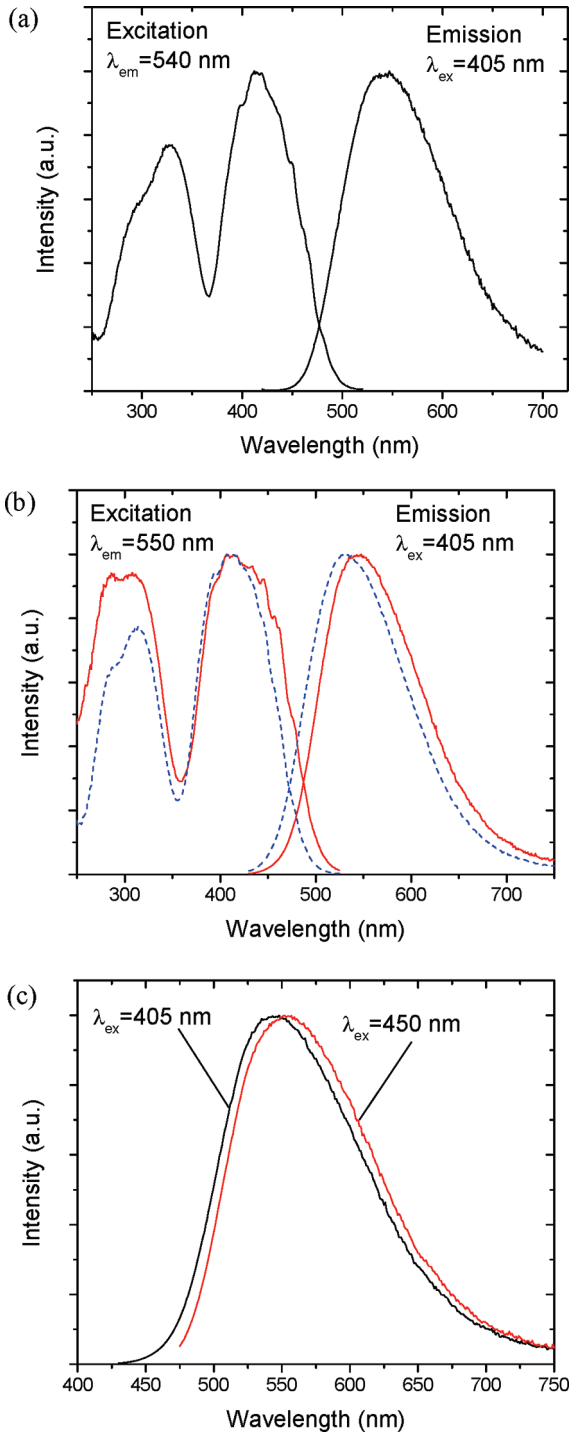

Figure 3. (a) Excitation (λ_{em} = 540 nm) and emission spectra (λ_{ex} = 405 nm) for $(Sr_{0.98}Na_{0.01}Ce_{0.01})_3Al_{0.25}Si_{0.75}O_{4.75}F_{0.25}$; (b) emission ($\lambda_{ex}$ = 405 nm) and excitation (λ_{em} = 550 nm) spectra for $(Sr_{0.895}Ca_{0.1}Ce_{0.005})_3Al_{0.6}Si_{0.4}O_{4.415}F_{0.585}$ (dashed line) and $(Sr_{0.595}Ca_{0.4}Ce_{0.005})_3Al_{0.6}Si_{0.4}O_{4.415}F_{0.585}$ (solid line); and (c) emission spectra (λ_{ex} = 405 nm and λ_{ex} = 450 nm) for $(Sr_{0.595}Ca_{0.4}Ce_{0.005})_3Al_{0.6}Si_{0.4}O_{4.415}F_{0.585}$. The sharp lines from 440 to 500 nm in the excitation spectra are instrument artifacts from the Xe lamp source.

quenching of $Sr_3AlO_4F:Ce^{3+}$ and the phosphors with lower levels of Si^{4+}/O^{2-} (Figure 2), we initially propose that Ce^{3+} ions in these phosphors require only one F^- anion in their local coordination for significant improvements in their high-temperature performance.

The room-temperature QE (λ_{ex} = 450 nm) of these phosphors is approximately equivalent to commercial Ce^{3+}-doped garnet phosphors with QEs greater than 80%. In addition, the phosphor QE at room and elevated temperature remains generally constant within $(Sr_{1-x-y}Ca_xCe_y)_3Al_{1-z}Si_zO_{4+3y+z}F_{1-3y-z}$ compositions for $x < 0.5$, $y = 0.005$, and $z < 0.5$ (Figure 2a). In these phosphors, we observe the onset of room temperature concentration quenching when the Ce^{3+} concentration (y) is greater than 0.01. There is also additional thermal quenching at higher Ce^{3+} concentrations; compositions with $x < 0.5$, y = 0.01, and $z = 0.4$ have I(150 °C)/I(RT) = 0.80. The general behavior of enhanced thermal quenching at higher Ce^{3+} concentration is similar to observations in YAG:Ce^{3+}[29] and the detailed mechanism behind this quenching at high temperatures is a topic for further work. However, for Ce^{3+} concentrations of y = 0.005, the combined substitution of Ca^{2+} and Si^{4+}/O^{2-} in the Sr_3AlO_4F system lead to efficient Ce^{3+} phosphors whose excitation allow them to be used with 385−460 nm InGaN LEDs (Figure 3b), a yellow-green emission band (Figure 3c), and < 15% loss in quantum efficiency at 150 °C (Figure 2). Although this performance is promising and there is a reasonable correlation with phosphor composition, our arguments on the changes in the relative energy position of the Ce^{3+} $5d^1$ level versus the $4f^1$ ground state and the host conduction band with composition are qualitative because the local coordination (including charge compensation) for Ce^{3+} centers in these materials (vide infra) is not explicitly known.

The broadening of the Ce^{3+} excitation band in $(Sr_{0.595}Ca_{0.4}Ce_{0.005})_3Al_{0.6}Si_{0.4}O_{4.415}F_{0.585}$ is assigned to multiple Ce^{3+} centers that are present in this host. We believe that the vast majority of Ce^{3+} ions substitute into the 8-coordinated 8*h* site and that multiple Ce^{3+} centers arise from anion and cation disorder (Table 2). The assumption of multiple Ce^{3+} centers from disorder instead of occupation of the 10-coordinated 4*a* site is supported by the analysis of Sr_2REAlO_5 compositions that does not give evidence for occupation of the 10-coordinated 4*a* site by RE^{3+} ions.[23,30] The presence of multiple Ce^{3+} centers leads to inhomogeneous broadening of the Ce^{3+} emission with a redshift in the emission spectrum at lower energy excitation (Figure 3c). Energy transfer between high- and low-energy Ce^{3+} ions also occurs in these phosphors, as with $Sr_3AlO_4F:Ce^{3+}$ at high Ce^{3+} concentrations.[14] This is demonstrated by the emission wavelength dependence of the decay profiles (λ_{ex} = 394 nm) (Figure 4a). At short emission wavelengths, the decay profile is multiexponential with initial components that are faster than typical Ce^{3+} decay times of 40−80 ns. In contrast, at longer emission wavelengths (λ_{em} = 580 nm), there is an initial build-up with a time constant of ~10 ns followed by a single exponential decay with a decay time of 75 ns. These observations are consistent with energy transfer between Ce^{3+} centers with different energies for their lowest-energy $4f^1 \rightarrow 5d^1$

(29) Bachmann, V.; Ronda, C.; Meijerink, A. *Chem. Mater.* **2009**, *21*, 2077.
(30) Drofenik, M.; Golic, L. *Acta Crystallogr., Sect. B* **1979**, *35*, 1059.

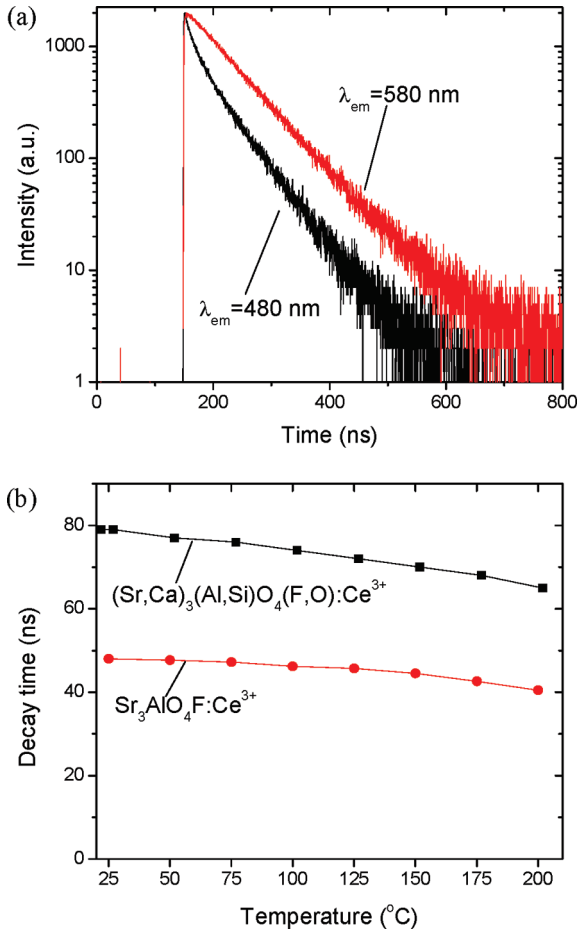

Figure 4. (a) Decay profile versus emission wavelength (λ_{ex} = 394 nm) for $(Sr_{0.595}Ca_{0.4}Ce_{0.005})_3Al_{0.6}Si_{0.4}O_{4.415}F_{0.585}$; and (b) decay time versus temperature for $(Sr_{0.599}Ca_{0.4}Ce_{0.001})_3Al_{0.6}Si_{0.4}O_{4.403}F_{0.597}$ (λ_{ex} = 520 nm; λ_{em} > 700 nm) and $(Sr_{0.98}Na_{0.01}Ce_{0.01})_3AlO_4F$ (λ_{ex} = 394 nm; λ_{em} = 490 nm). The drawn lines in panel b are only to guide the eye.

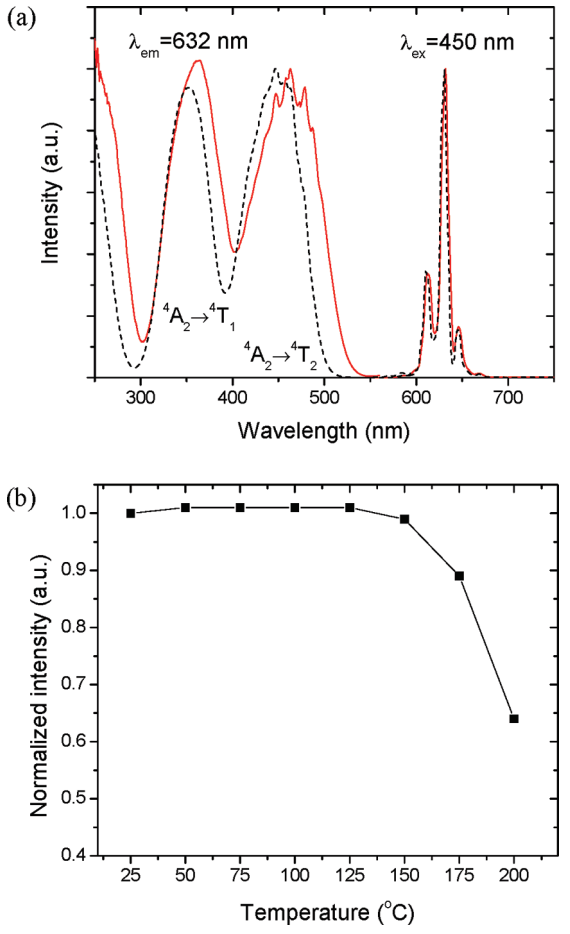

Figure 5. (a) Excitation (λ_{em} = 632 nm) and emission spectra (λ_{ex} = 450 nm) for $K_2TiF_6:Mn^{4+}$ (solid line) and $K_2SiF_6:Mn^{4+}$ (dotted line). The sharp lines from 440 to 500 nm in the excitation spectrum are instrument artifacts from the Xe lamp source. (b) Relative intensity versus temperature (λ_{ex} = 450 nm) for $K_2TiF_6:Mn^{4+}$. The drawn line in panel b is to guide the eye.

transition and are similar to other LED phosphors with intrinsic disorder.[31]

The disorder in this phosphor complicates the analysis of luminescence quenching in $(Sr,Ca)_3(Al,Si)O_4(O,F):Ce^{3+}$ since multiple Ce^{3+} centers are excited/detected when the excitation is at the absorption maximum. To isolate a limited population of Ce^{3+} centers, we excited a $(Sr_{0.599}Ca_{0.4}Ce_{0.001})_3Al_{0.6}Si_{0.4}O_{4.403}F_{0.597}$ (nominal) sample in the green tail of the excitation spectrum (λ_{ex} = 520 nm) with detection in the red tail of the emission spectrum (λ_{em} > 700 nm). The reduction in decay time versus temperature for samples with and without Ca^{2+} and Si^{4+}/O^{2-} substitution is in good agreement with relative intensity versus temperature measurements (Figure 2). Although the local coordination for these Ce^{3+} centers is not exactly known, the small reduction in decay time at high temperatures further demonstrates that the efficiency of Ce^{3+} centers in these phosphors can be high at room and elevated temperatures.

3.3. Luminescence of Mn^{4+}-Doped Fluorides and LED Lamp Testing. Warm-white lamps require green/yellow-green and red spectral components, and narrow-line red phosphors simultaneously optimize both LER and CRI.[2] In discharge-based fluorescent lighting, two activator ions are used for narrow-line emission, Eu^{3+} and Mn^{4+}. Eu^{3+} has only spin and parity forbidden transitions that overlap with blue and violet InGaN LED radiation. The weak Eu^{3+} absorption leads to severe scattering losses when incorporating typical Eu^{3+}-doped phosphors into LED packages. It is also difficult to sensitize Eu^{3+} emission by either Ce^{3+} or Eu^{2+} due to quenching from a metal−metal charge transfer (MMCT) state.[32] In contrast, Mn^{4+}-doped phosphors have a spin-allowed, parity-forbidden $^4A_2 \rightarrow {}^4T_2$ transition that has sufficient absorption of blue and/or violet LED radiation. In fluoride hosts such as K_2TiF_6, the $^4A_2 \rightarrow {}^4T_2$ absorption transition peaks at ~460 nm with the $^2E \rightarrow {}^4A_2$ red line emission peaking at ~632 nm (Figure 5a).[15] Although the position of the $^2E \rightarrow {}^4A_2$ line emission remains generally constant for compositional modifications, the $^4A_2 \rightarrow {}^4T_2$ absorption band can be tuned through compositional modifications (Figure 5a). These basic spectral characteristics can be explained using the Tanabe-Sugano diagram for d^3 ions[33] because the position of the $^4T_2$ level is influenced by the crystal field splitting (and therefore

(31) Setlur, A. A.; Heward, W. H.; Gao, Y.; Srivastava, A. M.; Chandran, R. G.; Shankar, M. V. *Chem. Mater.* **2006**, *18*, 3314.
(32) Blasse, G. *Struct. Bonding* (*Berlin*) **1991**, *76*, 153.
(33) Tanabe, Y.; Sugano, S. *J. Phys. Soc. Jpn.* **1954**, *9*, 753.

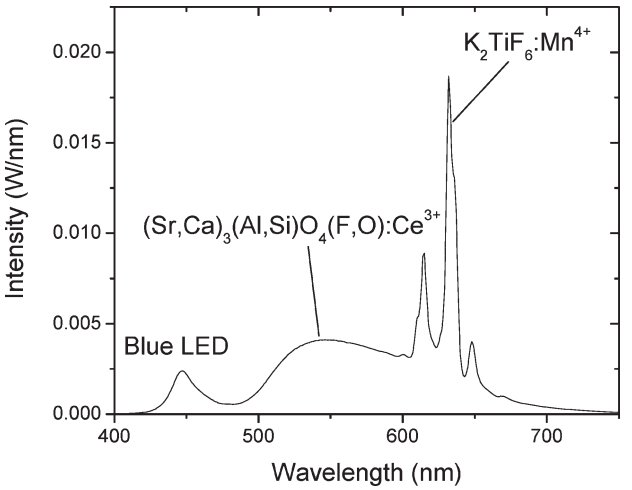

Figure 6. Spectrum of LED lamp using $(Sr_{0.595}Ca_{0.4}Ce_{0.005})_3Al_{0.6}Si_{0.4}O_{4.415}F_{0.585}$ and $K_2TiF_6:Mn^{4+}$ phosphors in combination with 450 nm LEDs in a remote phosphor configuration.

$Mn^{4+}-F^-$ bond lengths),[15] whereas the position of the ^2E level has a weak dependence on the crystal field splitting.

The QEs of $K_2TiF_6:Mn^{4+}$ and $K_2SiF_6:Mn^{4+}$ are comparable to commercial Ce^{3+}-doped garnets, and the quenching of these phosphors at 150 °C is less than 5% (Figure 5b), as previously reported.[15] These Mn^{4+} phosphors could be susceptible to saturation-based quenching in some LED packages[34] because their decay times are ~5.5 and ~8 ms for $K_2TiF_6:Mn^{4+}$ and $K_2SiF_6:Mn^{4+}$, respectively. However, saturation-based quenching can be virtually eliminated with a remote phosphor configuration[18,19] that reduces the incident radiation flux on these phosphors.

The combination of blue LED radiation, yellow-green emission from $(Sr_{0.595}Ca_{0.4}Ce_{0.005})_3Al_{0.6}Si_{0.4}O_{4.415}F_{0.585}$, and red line emission from $K_2TiF_6:Mn^{4+}$ gives high-CRI (>90), low-CCT (<3200 K) white lamps with a LER greater than 330 lm/W_{rad} (Figure 6). To assess phosphor performance in LED lamps, we normalized the lamp output by the blue LED optical power for a metric of lumens per watt of blue radiation (lm/W_{blue}). In our lamp configuration, this metric for cool-white lamps (CCT = 5000−6500 K, CRI = 70−80) using YAG:Ce phosphors is 210−220 lm/W_{blue}. Because the warm-white phosphor blend reported here has both high QEs and LERs, this metric for the oxyfluoride/fluoride phosphor blends in this lamp configuration is ~180−185 lm/W_{blue}, or ~85% of the cool-white value at a warm-white color temperature (CCT = 3088 K) and high color rendering (CRI = 90) (Figure 6). For our three LED package, this translates into warm-white lamps with efficacy of 82 lm/W (pulsed) with a total lumen output of 270 lm at 350 mA drive current and CIE (*x*,*y*) values of (0.441,0.423). The special R_9-R_{14} color indices[35] are all above 60 with a deep red R_9 special color index of 92. In addition, this lamp also has a color quality score[36−38] (CQS) of 90, so the color quality is still high with this new metric for color rendering. The high color rendering of this lamp therefore shows the potential to directly replace traditional light sources while retaining high efficacies.

4. Conclusions

In this report, we discuss the structural and luminescence properties of $(Sr,Ca)_3(Al,Si)O_4(O,F):Ce^{3+}$ yellow-green and $K_2TiF_6:Mn^{4+}$ red phosphors that can meet efficacy and color-quality requirements for future LED-based light sources. These oxyfluoride and fluoride phosphors are used for CRI = 90, warm-white LED lamps that reduce the efficacy gap between cool-white and warm-white LED packages by at least 50%. Apart from reducing the efficacy gap between cool-white and warm-white LED packages, these results further demonstrate the potential for alternate phosphor systems beyond typical garnet, nitride, and oxynitride phosphors that are used in LED lighting. If the long-term LED efficacy goal of 228 $lm/W_{electrical}$ for cool-white LEDs[1] is reached, the phosphor systems reported here could lead to 194 $lm/W_{electrical}$ warm-white LED packages that would enable replacements for incandescent (10−15 $lm/W_{electrical}$), halogen (15−30 $lm/W_{electrical}$), and compact fluorescent (60−70 $lm/W_{electrical}$) lamps. These future efficacy improvements will involve phosphor efficiency and lamp/package design optimization in combination with InGaN LED efficiency improvements.

Acknowledgment. The work presented in this report was partially supported by the U.S. Department of Energy through Contract DE-FC26-06NT42934 and by GE Lighting Solutions. This report was prepared as an account of work sponsored by an agency of the United States Government. Neither the United States Government nor any agency thereof, nor any of their employees, makes any warranty, express or implied, or assumes any legal liability or responsibility for the accuracy, completeness, or usefulness of any information, apparatus, product, or process disclosed, or represents that its use would not infringe privately owned rights. The views and opinions of authors expressed herein do not necessarily state or reflect those of the United States Government or any agency thereof. This research was performed in part at beamline X14A of the National Synchrotron Light Source, Brookhaven National Laboratory, Upton, NY. Research at the X14A beamline is partially sponsored by the U.S. Department of Energy, Office of Energy Efficiency and Renewable Energy, Vehicle Technologies Program, through the Oak Ridge National Laboratory's High Temperature Materials Laboratory User Program. The NSLS synchrotron facility is sponsored by the Office of Science, US Department of Energy under Grant DE-AC02-76CH00016.

Supporting Information Available: CIF file from the Rietveld refinement of $(Sr_{0.5925}Ca_{0.4}Ce_{0.0075})_3Al_{0.6}Si_{0.4}O_{4.4225}F_{0.5775}$, including the raw X-ray diffraction data used for this refinement. This material is available free of charge via the Internet at http://pubs.acs.org/.

(34) Setlur, A. A.; Shiang, J. J.; Happek, U. *Appl. Phys. Lett.* **2008**, *92*, 081104.
(35) *Method of Measuring and Specifying Colour Rendering Properties of Light Sources, Publication 13.3*; Commission Internationale de l'Eclairage: Vienna, 1995.
(36) Ohno, Y. *Proc. SPIE* **2004**, *5530*, 88.
(37) Ohno, Y. *Opt. Eng.* **2005**, *44*, 111302.
(38) Davis, W.; Ohno, Y. *Proc. SPIE* **2005**, *5941*, 59411G.